Nuclear Materials and Energy 12 (2017) 111–118

Contents lists available at ScienceDirect

Nuclear Materials and Energy

journal homepage: www.elsevier.com/locate/nme

Power exhaust by SOL and pedestal radiation at ASDEX Upgrade and JET

M. Bernert[a,*], M. Wischmeier[a], A. Huber[b], F. Reimold[b], B. Lipschultz[d], C. Lowry[c], S. Brezinsek[b], R. Dux[a], T. Eich[a], A. Kallenbach[a], A. Lebschy[a], C. Maggi[e], R. McDermott[a], T. Pütterich[a], S. Wiesen[b], JET contributors[f,1], the EUROfusion MST1 team[2], the ASDEX Upgrade Team

[a] Max Planck Institute for Plasma Physics, Boltzmannstr. 2, 85748 Garching, Germany
[b] Forschungszentrum Jülich GmbH, Institut für Energie- und Klimaforschung - Plasmaphysik, 52425 Jülich, Germany
[c] European Commission, B-1049 Brussels, Belgium
[d] University of York, York Plasma Institute, Heslington, York, YO10 5DD, United Kingdom
[e] CCFE, Culham Science Centre, Abingdon OX14 3DB, UK
[f] EUROfusion Consortium, JET, Culham Science Centre, Abingdon, OX14 3DB, UK

ARTICLE INFO

Article history:
Received 15 July 2016
Revised 27 November 2016
Accepted 22 December 2016
Available online 27 January 2017

ABSTRACT

Future fusion reactors require a safe, steady state divertor operation. A possible solution for the power exhaust challenge is the detached divertor operation in scenarios with high radiated power fractions. The radiation can be increased by seeding impurities, such as N for dominant scrape-off-layer radiation, Ne or Ar for SOL and pedestal radiation and Kr for dominant core radiation.

Recent experiments on two of the all-metal tokamaks, ASDEX Upgrade (AUG) and JET, demonstrate operation with high radiated power fractions and a fully-detached divertor by N, Ne or Kr seeding with a conventional divertor in a vertical target geometry. For both devices similar observations can be made. In the scenarios with the highest radiated power fraction, the dominant radiation originates from the confined region, in the case of N and Ne seeding concentrated in a region close to the X-point.

Applying these seed impurities for highly radiative scenarios impacts local plasma parameters and alters the impurity transport in the pedestal region. Thus, plasma confinement and stability can be affected. A proper understanding of the effects by these impurities is required in order to predict the applicability of such scenarios for future devices.

1. Introduction

Future fusion reactors require plasma scenarios with high dissipated power fractions in order to reduce the power flux on the divertor target plates. For ITER, about 85–90% of the exhaust power needs to be dissipated and for a possible DEMO reactor a fraction of more than 95% is required to meet the material limits [1,2]. With a sufficient reduction of the power flux to the divertor, the electron temperature in the divertor is reduced down to several eV, where atomic processes set in and volumetric recombination becomes efficient. In this detached state the particle and power flux to the targets reduces significantly.

The power dissipation consists of perpendicular transport, charge exchange losses and radiation losses, the latter usually being the biggest contribution. The radiated power can be increased by introducing seed impurities. These can be chosen to increase primarily the core (e.g. Kr, W) or scrape-off-layer radiation (e.g. N, Ne). In order to retain the enhanced energy confinement of the H-mode, the power flux across the separatrix has to stay above the L-H threshold [3]. Therefore, at ITER additional radiation in the core is not viable, while for DEMO the expected excess of alpha heating

* Corresponding author.
E-mail address: matthias.bernert@ipp.mpg.de (M. Bernert).

[1] See the Appendix of F. Romanelli et al., Proceedings of the 25th IAEA Fusion Energy Conference 2014, Saint Petersburg, Russia

[2] See http://www.euro-fusionscipub.org/mst1.

http://dx.doi.org/10.1016/j.nme.2016.12.029

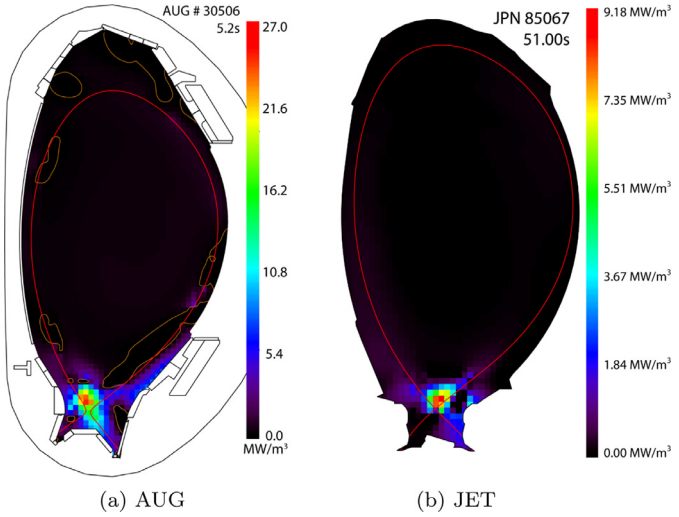

Fig. 1. Radiation distribution of nitrogen seeded discharges at AUG (#30506) and JET (JPN 85067) in the detached state.

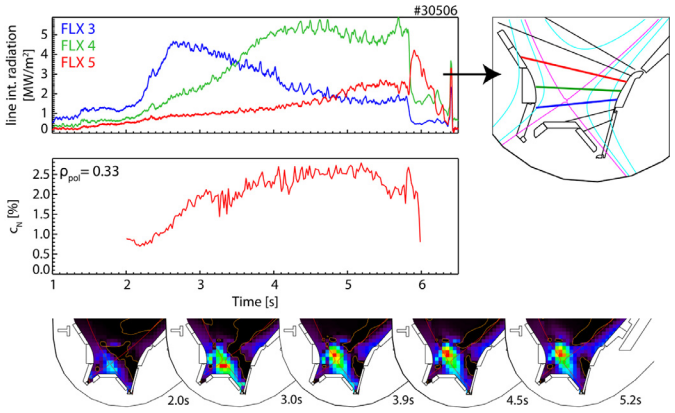

Fig. 2. Evolution of radiation around X-point, line of sight measurements (top), central nitrogen concentration (middle) and temporal evolution of tomographic reconstruction (bottom).

above the H-mode threshold allows (and requires) significant core radiation[4].

High radiation scenarios with different seed impurities were tested at two of the all-metal tokamaks, ASDEX Upgrade (AUG) and JET. These experiments aimed to demonstrate power exhaust at highest heat fluxes. The dominant parameter determining these heat fluxes is the ratio of the power flux over the separatrix P_{sep} and the major radius of the plasma R [5]. For ITER, this is in the range of $P_{sep}/R \approx 15$ MW/m and for DEMO expected to be in the range of 15–20 MW/m [1]. At AUG, values of up to $P_{sep}/R = 12$ MW/m were achieved, while at JET experiments were limited to about 5 MW/m.

This publication compares the observations at both machines and the impact of the various seed impurities on the plasma scenarios. It is ordered by the different seed impurities used, showing for both devices nitrogen seeding in Section 2, neon seeding in Section 3 and krypton seeding in Section 4. Section 5 compares the observations at both devices and Section 6 gives a summary and short outlook.

2. Nitrogen seeding

The use of nitrogen for divertor cooling is a well established technique [6]. It is commonly observed that the energy confinement time of the plasma is increased with the injection of nitrogen in an all-metal device [7]. At the same time, the N seeding is observed to alter the ELM characteristics, increasing their frequency and decreasing the relative energy loss [8].

Fig. 1a shows a tomographic reconstruction of the radiation distribution in AUG discharge #30506, where 18MW of heating power are applied at a constant N seeding rate. The normalized confinement following the ITER physics base scaling [9] is around $H_{98} = 0.9$ at up to 95% of the Greenwald density. In between the type-III ELMs, the divertor is in a pronounced detached state [10], where the particle flux onto the target is significantly reduced for about 10cm along the target. The radiated power fraction ($f_{rad} = P_{rad}/P_{heat}$) in this discharge is around 75%, while in discharges with lower heating power (e.g. AUG #29383) up to 90% of the heating power is radiated in the detached state.

In Fig. 1b a tomographic reconstruction of JET pulse 85067 is shown, where also 18MW of heating power are applied. The plasma is in a ELM-less H-mode, the confinement is around $H_{98} = 0.7$ at 90% of the Greenwald density. The divertor is in a fully detached state and the radiated power fraction at about 75%, the maximum observed at JET [11]. Note, that in this condition no significant heat flux is measured at the divertor [12,13]. At a higher heating power (JPN 87201, $P_{heat} = 27$ MW), the plasma is in a type-I ELMy H-mode but shows similar values of confinement and radiated power fraction as at 18MW.

The comparison in Fig. 1 shows that for both devices, in N seeded detached discharges, the dominant radiation is emitted by a small region inside the confined region, above the X-point. In both cases, about 5MW are radiated from this region, which is about 40% of the total radiation for JET and AUG.

For AUG, this so-called X-point radiator is consistently observed in the N seeded detached condition, not only at highest heating powers [14]. Such a local radiator inside the confined region can also be reproduced by modeling with the SOLPS code package [15,16].

Fig. 2 shows the temporal evolution of the location of the X-point radiator in discharge AUG #30506, where a constant N seeding rate is applied. This constant seeding leads to a slow increase of the N concentration in the confined plasma due to the residence time of nitrogen in the vacuum chamber. The X-point radiator develops in the region of the X-point and with increasing N concentration moves upwards inside the confined region. It appears to be very localized and not significantly elongated along the magnetic field lines.

The intense radiation in this region indicates a strong reduction of the local temperature to values of 10–100eV, where N radiates efficiently. Electron temperatures of only a few eV are indicated by the SOLPS modeling and by the observation of deuterium line radiation in the region below the X-point radiator. However, there is no direct measurement of the electron temperature in this region available yet. Such a local reduction of the electron temperature might represent a so-called radiation condensation, where the characteristics of the impurity radiation lead to a strong cooling down to the temperature of the most efficient radiation. This leads to a density increase in this region and a further amplification of the radiation losses. This indicates a similarity of the X-point radiator to the MARFE phenomenon [17]. However, the operation with such a X-point radiator does not lead to an unstable plasma, as it is usually observed with MARFEs in tokamaks with carbon as first wall material. As shown in Fig. 2, this radiator can exist for several seconds and modulations by ELMs and heating power trips do not lead to an immediate end of the discharge.

Such strong poloidal asymmetries of radiation and electron temperature might be unexpected for the confined region of the plasma. However, the X-point region has a high flux expansion

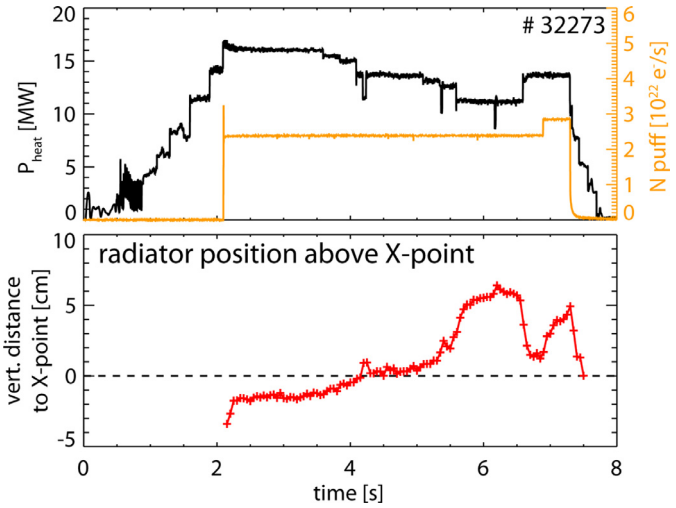

Fig. 3. Vertical position of the radiator relative to the X-Point in AUG #32273 with the modulation of heating power and N seeding (top).

and, thus, inside the confined region, a long connection length to the midplane. Therefore, poloidal temperature gradients result in rather low parallel temperature gradients. This temperature gradient drives a power flux into the radiating region, which can be sustained by the radial power flux into the specific flux surface, and which stabilizes the temperature in this region. As the connection length is strongly changing at the X-point (if moving vertically upwards), the region of intense radiation might be determined by a local equilibrium between power flux driven into the region (determined by the parallel temperature gradient) and the radiated power. This can also be an explanation of the observed vertical movement of the X-point radiator.

Using the lines of sight of the AXUV diode diagnostic [18], the vertical location and extend of the X-point radiator can be tracked. Fig. 3 shows the vertical position relative to the X-point for discharge AUG #32273. By a reduction of heating power, this radiator moves further inside the confined region. The innermost position shown in Fig. 3 corresponds to $\rho_{pol} \approx 0.9975$. With an increase of the heating power, the equilibration point of the radiator moves closer to the X-point. The increase of the N seeding levels leads again to an inward movement. If the radiator moves too far inside the confined region, a disruption is triggered (e.g. in AUG #32274). Similar to observations of MARFEs at the two devices with carbon as first wall material [19,20], the radiator moves upwards along the high-field side and most likely triggers a disruptive 2/1-island through the shrinking of the current channel by the edge cooling.

The X-point radiator is observed in both devices, at AUG and JET, indicating that it is a general operational regime for devices with a full-metal wall. For both devices the radiator is, in detached conditions, inside the confined region and dissipating a significant fraction of the injected power by radiation. It still needs to be evaluated, in which way this radiation impacts the power flux over the separatrix, which determines the access to H-mode, and how the plasma confinement of such a scenario is affected.

3. Neon seeding

Neon is a promising candidate as an edge radiating impurity for future reactor scenarios. It radiates dominantly at temperatures of about 50eV, which exist in the SOL. It does not trap tritium in the device as predicted for N, which potentially forms tritiated ammonia [21]. Therefore, high radiation scenarios with Ne instead of N seeding were tested at both devices, AUG and JET.

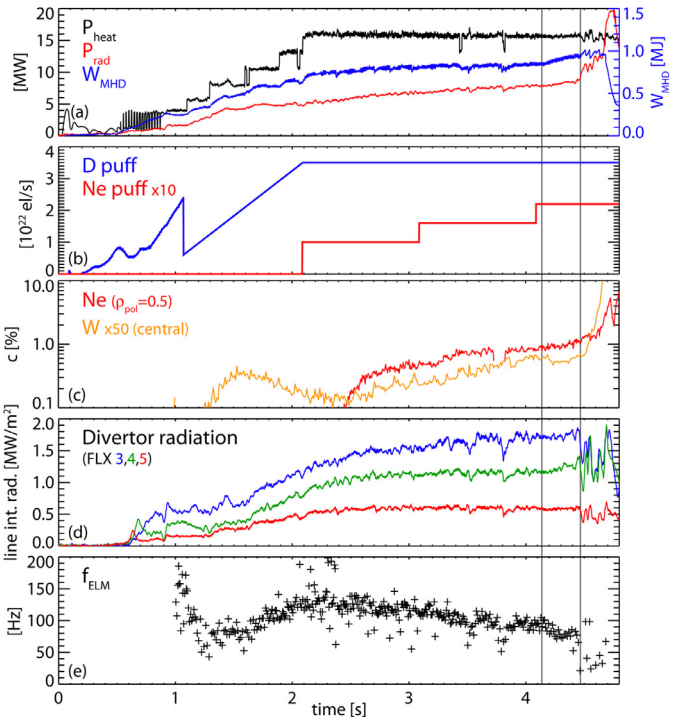

Fig. 4. Time traces of Ne seeded discharge AUG #32272. The gray lines indicate when the confinement starts to increase and when the ELM frequency drops, respectively.

3.1. Ne seeding at AUG

Fig. 4 shows time traces of a Ne seeded discharge #32272 at AUG. The Ne seeding level is increased in three steps. The first two levels lead to a slight increase of the central Ne concentration and the overall radiation level. However, the divertor radiation (Fig. 4(d)) is only marginally affected by the injected neon, showing that Ne does not increase the divertor radiation to required levels for efficient power exhaust (compared to N in Fig. 2). The presented discharge is ended by a central accumulation of tungsten, which results from changes in pedestal transport and ELM frequency caused by the Ne seeding, as described below.

The injection of Ne leads to an improvement of the confinement, here seen at 4.1s, similar to the observations made with nitrogen. Unlike for N, where the pedestal top temperature is increased and, thus, leads to the confinement improvement [22], with Ne the pedestal top density is increased. Edge kinetic profiles before and after the confinement improvement are shown in Fig. 5(a).

The ratio of the neoclassical radial drift and diffusion coefficients for impurities, shown in Fig. 5(b), is calculated with the NEOART code [23]. The neoclassical inward drift, which dominates the pedestal impurity transport in between ELMs [24], increases significantly for Ne as well as for tungsten with the increased density gradient. This leads to an increase of the peaking factor of tungsten at the pedestal

$$F_W = \frac{n_W(\rho_{pol} = 0.97)}{n_W(\rho_{pol} = 1)} = \int_{1.0}^{0.97} \frac{v}{D} dr$$

[25] from 5 to 35.

Furthermore, the ELM frequency is steadily reducing during the Ne seeding (Fig. 4(e)). This is the typical behaviour of type-I ELMs due to the reduction of the heating power [26]. In the present case, the central radiation of Ne reduces the actual power flux over the separatrix and thus leads to the reduction of ELM frequency. By

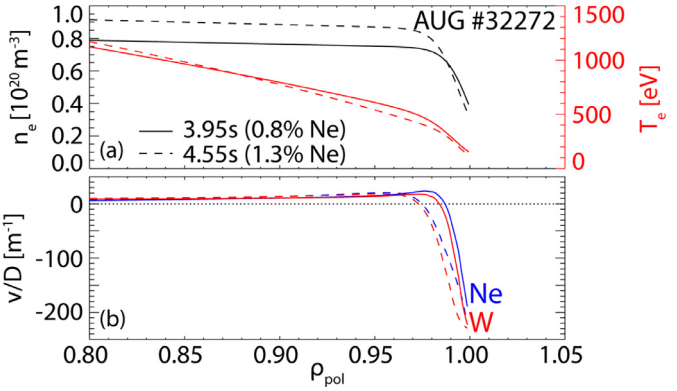

Fig. 5. Top: Edge profiles of electron density and temperature before and after the confinement improvement. Bottom: NEOART calculation of the neoclassical impurity transport at the pedestal.

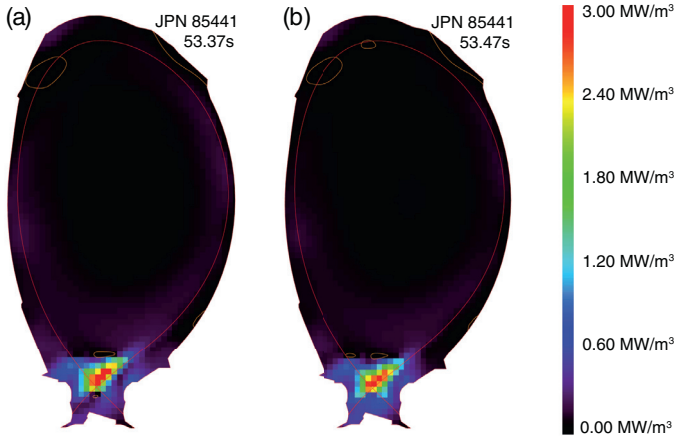

Fig. 6. Radiation distribution of the Ne seeded discharge JPN 85441. (a): H-mode, detached state; (b) L-mode, attached state.

the decrease in the ELM frequency, the effect of impurity flushing by ELMs [24] is significantly reduced.

Both effects together, namely the increased neoclassical inward transport and the reduced ELM flushing, lead to a strong, self-amplifying increase of the impurity concentration in the confined plasma and, thus, the collapse of the discharge.

The lack of efficient divertor cooling and the above mentioned effects of impurity transport make it impossible to study power exhaust with Ne seeding at the tested AUG parameters. In future devices the pedestal impurity transport is expected to be very different from current experiments due to the higher pedestal temperature gradients and lower density gradients. The temperature screening of impurities increases and the density gradient driven inward pinch reduces [27]. Therefore, the application of Ne seeding for power exhaust in such devices might still be possible.

3.2. Ne seeding at JET

At JET, Ne seeding to high radiated power fractions (f_{rad} > 50%) leads to a dithering between ELM-less H-modes and L-modes and a confinement of $H_{98} \leq 0.8$ [11]. In these cases the dominant radiation is emitted from the region inside the X-point, similar to the observations with N seeding. With the dithering between H- and L-mode, the divertor goes from a detached (H-mode) to attached (L-mode) state. In H-mode the radiation is concentrated at the region just inside the X-point while in L-mode the radiation is more diffuse in the divertor and increased in the SOL (see Fig. 6).

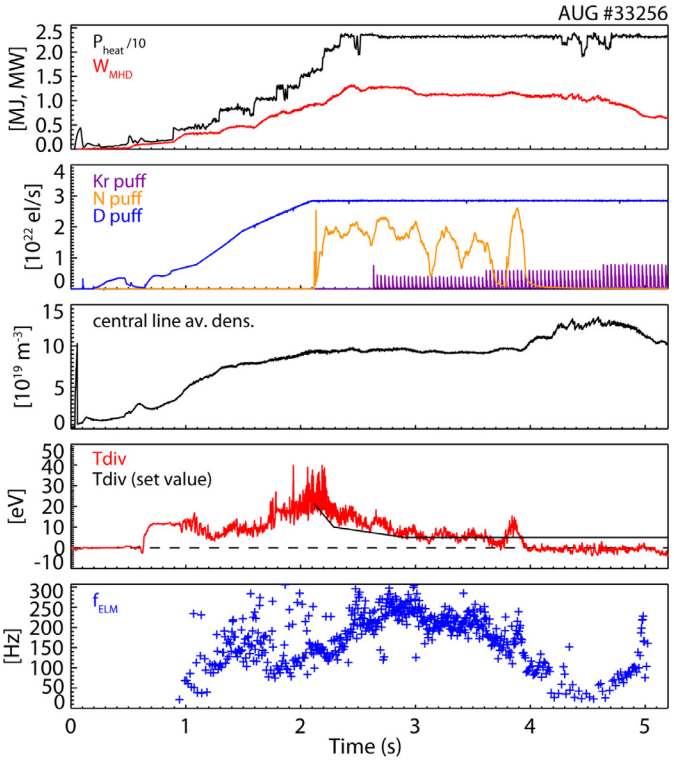

Fig. 7. Time traces of Kr seeded discharge AUG #33256.

The transitions between H- and L-mode indicate that the central radiation losses by Ne reduce the power flux over the separatrix below the L-H power threshold. In L-mode, the power flux over the separatrix is about 1MW higher than in H-mode. This difference might determine the change between H- and L-mode, however, the power flux in H-mode is with 9.5MW still above the L-H threshold scaling of about 8.7MW.

The dithering between H- and L-mode makes Ne seeding also not applicable for power exhaust scenarios at JET for the tested heating power of about 19MW. With an external heating of more than 22MW, the plasma might stay in H-mode and Ne could be further tested as a SOL and divertor radiator. However, such heating powers were not available for these experiments.

4. Krypton seeding

Krypton has a high radiation efficiency at electron temperatures of about 300eV. Thus, it is expected to create strong radiation in the pedestal region inside the separatrix, as it is required for future fusion reactors. Additionally, at 15eV the cooling factor of Kr has another peak, therefore, also increased radiation in a detached divertor can be expected.

4.1. Kr seeding at AUG

Fig. 7 shows time traces of discharge AUG #33256, where Kr seeding is applied. Very low seeding rates of Kr are required (Γ_{Kr} < 2 10^{21} *l/s*), therefore, a gas puff modulation scheme is applied in order to achieve reliable particle fluxes from the gas valves. There is no effect seen by this modulation, indicating that the transport time scale of Kr is above 30ms. In the presented discharge, a N puff was applied by a real time feedback [6] to keep the electron temperature at the outer divertor target around 5eV. The additionally injected Kr is stepwise replacing the N puff.

With the first step, there is only a small reduction on the averaged N seeding rate in order to keep the divertor temperature

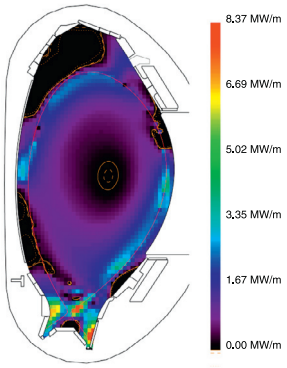

Fig. 8. Radiation distribution (ELM averaged) with dominant Kr radiation for AUG #33256. The radiated power fraction is up to 90% and a radiating ring evolves at the pedestal. Such a radially narrow structure, which is most likely poloidally symmetric, cannot fully be reconstructed by the tomographic inversion (see Fig. 9 for details). The radiation in the divertor legs is dominated by ELM induced radiation.

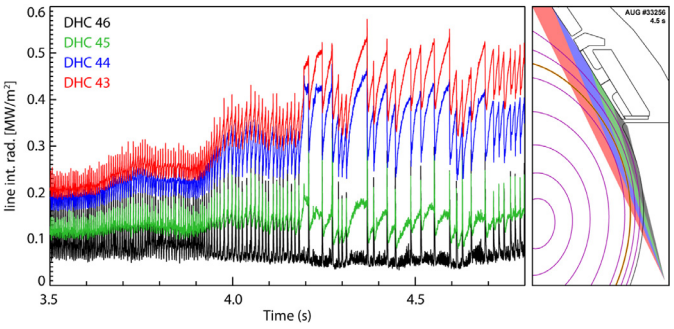

Fig. 9. Left: Time traces of AXUV diode measurements at the pedestal region for AUG #33256. Right: Viewing volume of AXUV channels.

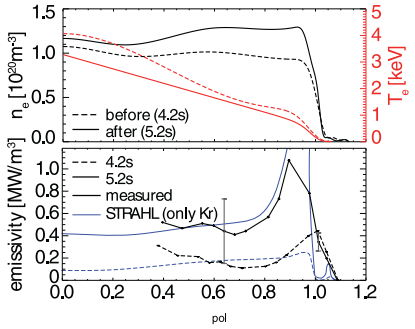

(a) Discharge with high heating power (AUG #30503, $P_{heat} = 19$ MW, $I_P = 1.2$ MA), plasma stored energy stays constant.

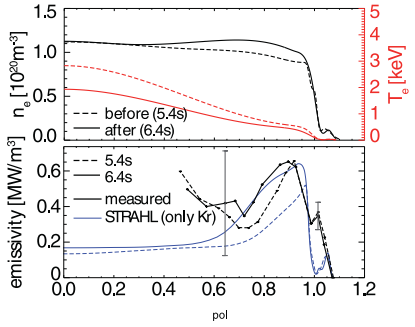

(b) Discharge with medium heating power (AUG #31648, $P_{heat} = 13.7 - 10.8$ MW, $I_P = 1.0$ MA), stored energy reduces.

Fig. 10. Kinetic profiles (top) and radiation profiles (bottom, inverted from bolometry measurements and modeled by STRAHL [29]) for two discharges before and after the radiation is dominated by Kr. Adapted from [28].

constant. The ELM frequency reduces slightly as the power flux over the separatrix is reduced by an increased central radiation. The drop in plasma stored energy at 3s is caused by an internal 3/2 NTM, which develops at the high beta normalized of 2.7. This reduces the stored energy by 10%, which remains stable later on. Other plasma parameters do not change significantly.

With the second level of Kr seeding, the divertor goes into the detached state ($T_{div} \approx 0$eV) and no further N seeding is required for divertor cooling. With Kr as dominant radiator, a radiating ring is forming around the pedestal region (see Fig. 8). The Kr radiation inside the confined region dissipates sufficient power to reduce the power fluxes onto the target plates to reach detachment. The radiated power fraction is up to 90%. This is observed with Kr concentrations of less than $5 \cdot 10^{-4}$ (Fig. 10,[28]). With the onset of detachment, the plasma density increases by more than 30%.

Fig. 9 shows the line integrated measurements of the pedestal radiation by AXUV diodes. The dominant radiation is emitted in the region of channel DHC44, which is dominantly measuring between $\rho_{pol} = 0.95 - 1$. This is identified by the strong signal increase from DHC45 to DHC44, but no further increase to DHC43. With the strong radiation inside the confined region, the ELM frequency reduces to 10–20Hz.

In Fig. 9 the strong modulation of the pedestal radiation by ELMs can also be seen. In between ELMs, the pedestal radiation increases rapidly, while the pedestal is strongly eroded by an ELM. This can be explained by a strong inward transport of Kr in between ELMs, created by an increased density pedestal as shown in Section 3.1. Kr is cooling the pedestal region and, thus, leading to a further increase of the density. This is a self-amplifying process and leads transiently to hollow density profiles. The Kr in the pedestal region is flushed out by ELMs and the pedestal radiation is decreased. After an ELM, Kr is again transported inside.

At high ELM frequencies, the balance of inward transport and ELM flushing of Kr could potentially lead to a quasi steady state scenario. However, as Kr increases the central radiation and by this reduces the power flux over the separatrix, the ELM frequency is inherently reduced and the net inward transport of Kr is increasing. This results in a very low ELM frequency and can lead to a (minor) radiative collapse of the plasma, seen in Fig. 7 at 4.8s. Attempts to keep a high ELM frequency e.g. by additional N injection showed that the effect of Kr on the ELM frequency is still dominating. Therefore, other means of ELM frequency control are required and not yet tested.

The impact of the Kr radiation on the confinement depends on the radial location of the radiation. Fig. 10 compares kinetic profiles and radiation profiles for two Kr seeded discharges with different heating powers. In the discharge with high heating power ($P_{heat} = 19$MW), the pedestal top temperature is reduced by the Kr radiation from 1.2keV to 800eV. The region of maximum emissivity of Kr stays inside the pedestal region and the stored energy of the plasma is observed to not be affected. For the STRAHL simulation, a Kr concentration of $5 \cdot 10^{-4}$ was assumed. This is well reproducing the radiated power measurements, even though no other impurities were included in the calculation, and, thus, indicates a upper threshold for the Kr concentration [28].

In the case with lower heating power ($P_{heat} = 10.5$MW), Kr leads to a reduction of the pedestal top temperature from more than 500eV to less than 400eV. In these cases the dominant Kr radiation shifts further inside the confined region and the con-

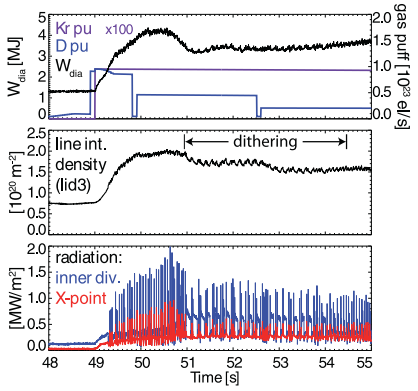

(a) JPN 90363

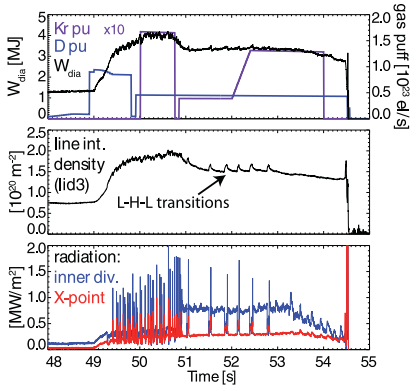

(b) JPN 90368

Fig. 11. Time traces of two JET discharges, showing the dithering between H- and L-mode.

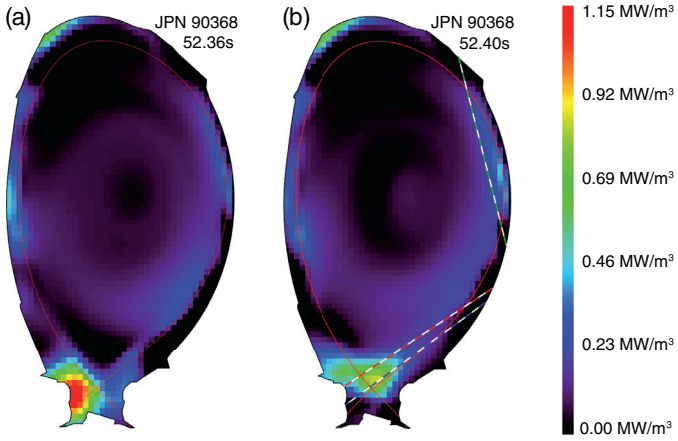

Fig. 12. Radiation distribution of the Kr seeded discharge JPN 90638 ((a): L-mode, attached state; (b) H-mode, detached state). The radiation forms a poloidal ring in the pedestal region (which cannot be fully reconstructed). The dashed lines indicate the LOS of bolometry used in Figs. 11 & 13.

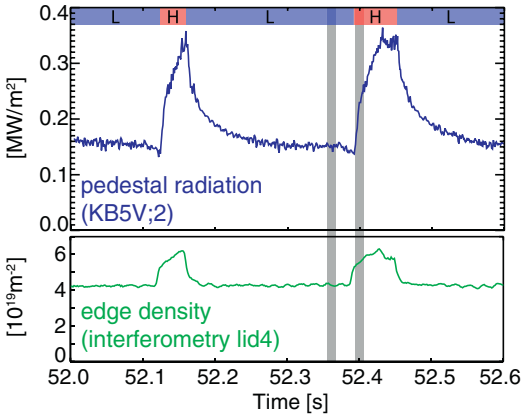

Fig. 13. Line integrated measurement of the pedestal radiation by bolometry channel KB5V/2 and pedestal density by interferometry channel lid4 in JPN 90368. The top bar indicates the L- or H-mode phase. The grey lines indicate the times of the tomographic reconstruction shown in Fig. 12.

finement is reduced by 20%. However, in these cases the ELM frequency remains high, mainly by a switching from type-I to type-III ELMs, and the discharge continues at the low confinement level. Both discharges appear to be stable on a short term. Nevertheless, the above mentioned impact of the central radiation on the ELM frequency leads to a collapse of the discharges.

4.2. Kr seeding at JET

Experiments with Kr seeding at JET shows similar characteristics like at AUG. Fig. 11 shows time traces of two Kr seeded discharges at a heating power of 18.5MW. With the Kr seeding the confinement reduces and a dithering between L- and H-mode is observed. The H-mode phases are characterized by an increase in density and stored energy and the development of the temperature pedestal. In the L-mode phases density and stored energy decrease. The divertor switches from a detached outer target and radiation at the X-point in H-mode to an attached target and radiation in the inner divertor volume in L-mode. The maximum radiated power fraction is in the order of 65%.

In JPN 90368 the plasma stays in L-mode after 53.3s. With the increased seeding, the divertor detaches and the pedestal radiation increases. This leads to a confinement reduction and finally to a disruption.

Fig. 12 shows the radiation distribution of an H- and an L-mode phase in JPN 90368. The radiation inside the confined region is strongly increased and creates a radiating ring in the pedestal region, similar to the observations at AUG. However, at JET the radiation in the divertor and at the X-point appears to be more pronounced than at AUG. Nonetheless, the ratio of divertor to main chamber radiation (split at z=-1.1m for JET and z=-0.66m for AUG) is for both devices about 1:3.

The transport of Kr plays a major role for the observed dithering between H- and L-mode. This can been seen in the pedestal radiation, shown in Fig. 13. The measurement of the pedestal density by an interferometry channel shows that the changes in radiation are not only due to density changes by the transitions between H- and L-mode, but are an indication for the Kr concentration in the pedestal region. In the H-mode phase the pedestal radiation increases rapidly. At this phase the Kr is most likely transported inwards due to the neoclassical inward transport over the pedestal. In L-mode the gradients relax again and the neoclassical inward drift reduced. Turbulence is most likely dominating the Kr transport in these phases and the Kr is flushed out of the confined region. Therefore, the pedestal radiation reduces again.

This change of Kr transport and, thus, radiation characteristics of the plasma changes the power flux over the separatrix by about 2MW (being higher in the L-mode). As the power flux is close to the L-H power threshold, such a change can determine whether the plasma is in L- or H-mode. The retarding effect of the Kr transport can then explain the dithering cycle of the Kr seeded discharges. Also the power flux into the divertor is altered by the two different regimes. With the reduced power flux of the H-mode, the divertor is detached between ELMs, while it is attached in L-mode.

The dithering between L- and H-mode is observed for seeding levels of $1 \cdot 10^{21}$el/s to $4 \cdot 10^{21}$el/s. JPN 90363 and 90368 show for different seeding levels similar transitions, the impact on the confinement is comparable (see Fig. 11). The change of the pedestal density and radiation between H- and L-mode as shown in Fig. 13 is in the similar range for both discharges. However, the cycle time between H- and L-mode changes; at JPN 90368, the L-mode phases are up to 0.4s long while in JPN 90363 they are shorter than 200ms. It appears that similar concentrations of Kr need to be achieved in the pedestal region to trigger the L-H or H-L transition. With a higher seeding level, this concentration is achieved faster in H-mode or takes more time to be removed in L-mode. In JPN 90368 from 52.3s on, the seeding is increased to $1.3 \cdot 10^{22}$el/s, which leads to a continuous L-mode phase. Note, however, that Kr seeding has a very slow response time and, thus, the time history of the seeding within the discharge also matters.

It might be possible to avoid the dithering by applying more heating power in order to stay significantly above the L-H power threshold. However, by the time of the execution of the experiments there was no additional heating power available and the data at higher heating powers is still pending.

5. Comparison between JET, AUG and other devices

Similar observations can be made for the high radiation scenarios at JET and AUG. With N seeding in both devices, strongly localized radiating regions inside the confined region above the X-point develop with the detachment of the divertor. For AUG, the confinement in these scenarios is only slightly reduced to $H_{98} \approx 0.9$, while at JET a stronger reduction to $H_{98} \approx 0.7$ is observed.

The scenarios compared at AUG and JET applied similar heating powers ($P_{heat} \approx 18 - 26$MW), regardless of the machine size or L-H power threshold. Normalized to these values, the scenarios at JET have about a factor of two less heating power than at AUG. As observed by the dithering between L- and H-mode in Ne and Kr seeded scenarios at JET, the power flux over the separatrix is for these scenarios close to the LH power threshold. In comparison to the results from AUG, it can be expected that the confinement for the high radiation scenarios at JET is higher if more heating power (in the range of 30–35MW) would be applied.

Despite the different first wall materials in both devices (only W at AUG, W and Be at JET), the wall material and wall conditioning does appear not to have a significant impact on the mechanisms behind the observed scenarios. The seed impurities were always applied for several shots in a row, and it can be expected that the wall depository for impurities was saturated. This can be seen by the reproducibility of such scenarios. Additionally, by the very high deuterium gas fueling and impurity seeding levels required for the highly powered discharges, any wall conditioning, such as boronisation, does not have a strong impact on the plasma scenarios.

Strong radiation inside the confined region is also reported by JT-60U in unseeded detached plasmas with carbon as first wall material [30]. Also at the compact all-metal tokamak Alcator C-Mod, radiation is observed in the vicinity of the X-point when applying strong N seeding [31,32], however the divertor is in the partial detached state and the peak radiation is localized outside the confined region. The application of Ne seeding leads to either reduced [31] or similar performance [32] than N seeding, but is not observed to cause similar instabilities like at AUG or JET. Ar and Kr seeding leads at Alcator C-Mod to a reduced confinement by the impact of the impurities on the core plasma [31].

6. Summary

High radiation scenarios with different seed impurities were tested at two of the all-metal tokamaks, ASDEX Upgrade and JET. High dissipated power fractions and detached targets were achieved at both devices. These scenarios apply impurities which were expected to radiate inside the confined region (Kr) or in the SOL and divertor region (N, Ne). However, in detached divertor conditions, independent of seed impurities species, the dominant radiation is emitted from the confined region, mainly close to the X-point.

At AUG, the highest radiated power fraction for stable scenarios at high heat fluxes ($P_{heat}/R \leq 15$ MW/m) is in the order of 90%. The H-factor in these scenarios is between 0.75 and 0.9 while densities up to 95% of the Greenwald density are achieved. At JET, the highest achieved radiated power fraction is 75%. However, in both devices no significant power flux was detected in the divertor.

The experiments at both devices show that impurity seeding can have a strong effect on local plasma parameters. A radiation condensation at the X-point which might lead to poloidal asymmetric radiation and temperature profiles inside the confined region. Therefore, it is not sufficient to solely apply the temperature dependent cooling coefficient of an impurity on existing temperature and density distributions for the design of future high radiation scenarios.

Furthermore, the experiments show that impurity transport, especially in the pedestal region, is an important parameter for the stability of high radiation scenarios. This can be seen for both devices with Kr seeding and for AUG also with Ne seeding. Both impurities affect the pedestal parameters and the impurity transport over the pedestal, which can lead to a self-amplification. Therefore, Ne and Kr seeding cannot be used for power exhaust studies at the tested AUG parameters, if no other means of impurity control, i.e. ELM pacing, are applied.

High radiation scenarios with detached targets are, nonetheless, a promising candidate to solve the challenge of power exhaust in future fusion reactors. The pedestal impurity transport is expected to be beneficial for such scenarios in these devices [27]. The application of Ar and of impurity mixes has to be tested further. The latter allows to tailor the radiation distribution in fusion plasmas and opens the possibility to optimize such scenarios for good confinement, stable scenarios and highest fusion gain.

Acknowledgment

This work has been carried out within the framework of the EUROfusion Consortium and has received funding from the Euratom research and training programme 2014-2018 under grant agreement No 633053. The views and opinions expressed herein do not necessarily reflect those of the European Commission.

References

[1] M. Wischmeier, High density operation for reactor-relevant power exhaust, J. Nucl. Mater. 463 (2015) 22–29. www.sciencedirect.com/science/article/pii/S0022311514010216.

[2] A.S. Kukushkin, H.D. Pacher, G.W. Pacher, V. Kotov, R.A. Pitts, D. Reiter, Consequences of a reduction of the upstream power SOL width in ITER, J. Nucl. Mater. 438 (2013) S203–S207. http://www.sciencedirect.com/science/article/pii/S0022311513000354 Supplement.

[3] Y.R. Martin, T. Takizuka, the ITPA CDBM H-mode Threshold Database Working Group, Power requirement for accessing the H-mode in ITER, J. Phys. Conf. Ser. 123 (1) (2008) 012033. http://stacks.iop.org/1742-6596/123/i=1/a=012033.

[4] H. Zohm, C. Angioni, E. Fable, et al., On the physics guidelines for a tokamak DEMO, Nucl. Fusion 53 (7) (2013) 073019. http://stacks.iop.org/0029-5515/53/i=7/a=073019.

[5] T. Eich, A.W. Leonard, R.A. Pitts, et al., Scaling of the tokamak near the scrape-off layer H-mode power width and implications for ITER, Nucl. Fusion 53 (9) (2013) 093031. http://stacks.iop.org/0029-5515/53/i=9/a=093031.

[6] A. Kallenbach, R. Dux, J.C. Fuchs, et al., Divertor power load feedback with nitrogen seeding in ASDEX Upgrade, Plasma Phys. Control. Fusion 52 (5) (2010) 055002. http://stacks.iop.org/0741-3335/52/i=5/a=055002.
[7] M.N.A. Beurskens, J. Schweinzer, C. Angioni, et al., The effect of a metal wall on confinement in JET and ASDEX Upgrade, Plasma Phys. Control. Fusion 55 (12) (2013) 124043. http://stacks.iop.org/0741-3335/55/i=12/a=124043.
[8] P.A. Schneider, E. Wolfrum, M.G. Dunne, et al., Observation of different phases during an ELM crash with the help of nitrogen seeding, Plasma Phys. Control. Fusion 56 (2) (2014) 025011. http://stacks.iop.org/0741-3335/56/i=2/a=025011.
[9] ITER Physics Expert Group on ConfinementTransport, ITER Physics Expert Group on Confinement Modelling, Database, ITER Physics Basis Editors, Chapter 2: plasma confinement and transport, Nucl. Fusion 39 (12) (1999) 2175. http://stacks.iop.org/0029-5515/39/i=12/a=302.
[10] A. Kallenbach, M. Bernert, M. Beurskens, et al., Partial detachment of high power discharges in ASDEX Upgrade, Nucl. Fusion 55 (5) (2015) 053026. http://stacks.iop.org/0029-5515/55/i=5/a=053026.
[11] A. Huber, M. Wischmeier, C.G. Lowry, et al., Impact of Strong Impurity Seeding on the Radiation Losses in JET with ITER-like Wall, in: Europhysics Conference Abstracts (Proc. of the 41th EPS Conference on Controlled Fusion and Plasma Physics, Berlin, 2014), 2014. http://ocs.ciemat.es/EPS2014PAP/pdf/P1.031.pdf, page P1.031.
[12] S. Devaux, C. Guillemaut, et al., Energy balance in JET, This conference, submitted to Nucl. Mater. Energy.
[13] C. Guillemaut, P. Drewelow, G.F. Matthews, et al., Evidence for enhanced main chamber wall plasma loads in JET ITER-like wall at high radiated fraction, This conference, submitted to Nucl. Mater. Energy.
[14] F. Reimold, M. Wischmeier, M. Bernert, et al., Divertor studies in nitrogen induced completely detached H-modes in full tungsten ASDEX Upgrade, Nucl. Fusion 55 (3) (2015a) 033004. http://stacks.iop.org/0029-5515/55/i=3/a=033004.
[15] F. Reimold, M. Wischmeier, M. Bernert, et al., Experimental studies and modeling of complete h-mode divertor detachment in ASDEX Upgrade, J. Nucl. Mater. 463 (2015b) 128–134. http://www.sciencedirect.com/science/article/pii/S002231151400960X.
[16] E. Sytova, I. Senichenkov, E. Kaveeva, et al., Analysis of impurity momentum balance and flows in the sol by solps-iter modelling, in: Europhysics Conference Abstracts (Proc. of the 43th EPS Conference on Controlled Fusion and Plasma Physics, Leuven, 2016), 2016. http://ocs.ciemat.es/EPS2016PAP/pdf/P1.054.pdf, page P1.054.
[17] B. Lipschultz, B. LaBombard, E.S. Marmar, et al., MARFE: an edge plasma phenomenon, Nucl. Fusion 24 (8) (1984) 977. http://stacks.iop.org/0029-5515/24/i=8/a=002.
[18] M. Bernert, T. Eich, A. Burckhart, et al., Application of AXUV diode detectors at ASDEX Upgrade, Rev. Sci. Instrum. 85 (3) (2014). http://scitation.aip.org/content/aip/journal/rsi/85/3/10.1063/1.4867662.
[19] J.A. Wesson, R.D. Gill, M. Hugon, et al., Disruptions in jet, Nucl. Fusion 29 (4) (1989) 641. http://stacks.iop.org/0029-5515/29/i=4/a=009.
[20] V. Mertens, M. Kaufmann, J. Neuhauser, et al., High density operation close to greenwald limit and h mode limit in ASDEX Upgrade, Nucl. Fusion 37 (11) (1997) 1607. http://stacks.iop.org/0029-5515/37/i=11/a=I10.
[21] M. Oberkofler, D. Alegre, F. Aumayr, et al., Plasma-wall interactions with nitrogen seeding in all-metal fusion devices: formation of nitrides and ammonia, Fusion Eng. Des. 98–99 (2015) 1371–1374. http://www.sciencedirect.com/science/article/pii/S092037961500071X.
[22] A. Kallenbach, M. Bernert, R. Dux, et al., Impurity seeding for tokamak power exhaust: from present devices via ITER to DEMO, Plasma Phys. Control. Fusion 55 (12) (2013) 124041. http://stacks.iop.org/0741-3335/55/i=12/a=124041.
[23] R. Dux, A.G. Peeters, Neoclassical impurity transport in the core of an ignited tokamak plasma, Nucl. Fusion 40 (10) (2000) 1721. http://stacks.iop.org/0029-5515/40/i=10/a=304.
[24] T. Pütterich, R. Dux, M.A. Janzer, R.M. McDermott, ELM flushing and impurity transport in the H-mode edge barrier in ASDEX Upgrade, J. Nucl. Mater. 415 (1) (2011) S334–S339. http://www.sciencedirect.com/science/article/pii/S0022311510005623, Proceedings of the 19th International Conference on Plasma-Surface Interactions in Controlled Fusion.
[25] T. Pütterich, R. Dux, E. Wolfrum, E. Viezzer, the ASDEX Upgrade Team, Impurity transport within an ELM-cycle at the edge transport barrier in ASDEX Upgrade, in: Europhysics Conference Abstracts (Proc. of the 36th EPS Conference on Controlled Fusion and Plasma Physics, Sofia, 2009), 2009. http://epsppd.epfl.ch/Sofia/pdf/P1_158.pdf, page P1.158.
[26] H. Zohm, Edge localized modes (ELMs), Plasma Phys. Control. Fusion 38 (2) (1996) 105. http://stacks.iop.org/0741-3335/38/i=2/a=001.
[27] R.M. Dux, A. Loarte, C. Angioni, D. Coster, E. Fable, A. Kallenbach, The interplay of controlling the power exhaust and the tungsten content in ITER, This conference, submitted to Nucl. Mater. Energy. http://dx.doi.org/10.1016/j.nme.2016.10.013.
[28] M. Bernert, F. Reimold, R. Dux, et al., High radiation scenarios with radiation inside the confined region at ASDEX Upgrade, in: Europhysics Conference Abstracts (Proc. of the 42nd EPS Conference on Controlled Fusion and Plasma Physics, Lisbon, 2015), 2015. http://ocs.ciemat.es/EPS2015PAP/pdf/P1.135.pdf, page P1.135.
[29] R. Dux, STRAHL User manual, Max-Planck-Institut für Plasmaphysik, Garching, 2006. IPP report 10/30.
[30] T. Nakano, H. Kubo, N. Asakura, K. Shimizu, H. Kawashima, S. Higashijima, Radiation process of carbon ions in JT-60U detached divertor plasmas, J. Nucl. Mater. 390–391 (2009) 255–258. http://www.sciencedirect.com/science/article/pii/S0022311509001081, Proceedings of the 18th International Conference on Plasma-Surface Interactions in Controlled Fusion DeviceProceedings of the 18th International Conference on Plasma-Surface Interactions in Controlled Fusion Device.
[31] J.A. Goetz, B.L. Bombard, B. Lipschultz, et al., High confinement dissipative divertor operation on Alcator C-Mod, Phys. Plasmas 6 (5) (1999) 1899–1906. http://scitation.aip.org/content/aip/journal/pop/6/5/10.1063/1.873447;jsessionid=q5wC3Vt1q97gFEfkDJ2wRLhT.x-aip-live-03.
[32] A. Loarte, J.W. Hughes, M.L. Reinke, et al., High confinement/high radiated power H-mode experiments in alcator C-Mod and consequences for international thermonuclear experimental reactor (ITER) q_DT=10 operation, Phys. Plasmas 18 (5) (2011). http://scitation.aip.org/content/aip/journal/pop/18/5/10.1063/1.3567547.